Acta Geodaetica et Geophysica
https://doi.org/10.1007/s40328-026-00511-7

RESEARCH

An integrated petrophysical–geological framework for reliable permeability prediction in carbonate reservoirs, bridging core and log scales

Abel Carrasquilla[1] · Heitor Lichotti[1] · Herson Rocha[2]

Received: 26 February 2026 / Accepted: 16 June 2026

Abstract

Heterogeneous carbonate reservoirs pose a significant challenge for accurate permeability prediction, crucial for reservoir characterization and production planning. This study addresses this challenge by presenting an integrated multi-method workflow that synergizes petrophysical rock typing with hydraulic flow unit (HFU) delineation. Applied to the post-salt Albian carbonate reservoir of the Linguado field in Brazil, the methodology transcends the limitations of standard empirical correlations. Porosity was initially assessed using wireline logs and then compared with laboratory sample data from boreholes LIN03 and LIN10. The acoustic, density, and neutron porosity values for LIN03 yielded Pearson correlation coefficients (R^2) of 0.29, 0.21, and 0.14, respectively. In contrast, LIN10 exhibited slightly better results with R^2 values of 0.51, 0.50, and 0.37. The consistency of the approach was confirmed across both wells, with the larger dataset from LIN10 yielding marginally stronger initial correlations, where the sonic porosity was selected for subsequent permeability estimates due to its relative superiority over other estimates. After addressing this initial challenge, a permeability estimate was calculated using Timur's empirical equation, yielding an R^2 of 0.12. This outcome underscores the need for more reliable models that can incorporate reservoir zoning based on lithofacies, flow zones, and hydrodynamic flow units. This categorized method led to the formulation of regression equations for each hydrodynamic flow unit. While refined analysis can achieve greater accuracy by integrating results from multiple assessment techniques, the hydrodynamic flow units proved critical for accurately evaluating permeability relative to laboratory results, demonstrating the effectiveness of this method. The permeability of LIN03 showed an $R^2 = 0.97$, whereas LIN10 presented an $R^2 = 0.98$. These values can be used to forecast possible flow zones in additional oilfield boreholes. An advanced step in estimation methodologies was reached when the provided methodology culminated in a linear regression analysis to estimate permeability inside each hydrodynamic flow unit of the post-salt reservoir in southeastern Brazil.

Keywords Petrophysical study · Integration of core data and well logs · Flow units' differentiation · Permeability evaluation · Albian carbonate reservoir

Extended author information available on the last page of the article

Published online: 06 July 2026

1 Introduction

Approximately 7% of Earth's surface is covered by carbonate rock, which contains nearly all the world's hydrocarbon reserves. These rocks host around 70% of the Middle East's extensive oilfields, which represent over 60% of global oil reserves and 40% of global natural gas reserves (Lucia et al. 2003; Lucia 2007). In contrast to siliciclastic reservoirs, carbonate rocks pose greater challenges for characterization due to their lithological complexity. They frequently undergo intense diagenetic processes, including cementation, dissolution, dolomitization, recrystallization, and biological activity (Gomes et al. 2008).

The recognition of these elements through petrophysical studies is essential for evaluating reservoir behavior, which is crucial for identifying flow units. These units represent different parts of a reservoir exhibiting similar flow characteristics. The identification of these units enables the evaluation of permeability, which estimates the efficiency with which fluids traverse a reservoir. This approach aids in identifying and characterizing reservoirs, predicting their performance, and optimizing production plans (Al-Tooqi et al. 2014).

Integrating geological and petrophysical data enables the development of a rock-fluid reservoir model. This investigation distinguishes between the rock types that make up reservoirs and those that do not. A petrophysical rock type (PRT) is a technique for classifying rocks based on their physical properties, particularly porosity (ϕ) and permeability (k). Understanding reservoir behavior relies heavily on certain properties, particularly in differentiating between pore geometry, mineral content, and specific fluid-flow characteristics. Analytical techniques play a vital role in developing flow models for reservoirs, as these models connect flow characteristics to the PRT (Amaefule et al. 1993). The models are based on several laboratory experiments with rock samples (Gomaa et al. 2006).

Experimental measures of ϕ and k, thin-sheet analysis, pore structure inspection with an electron microscope, capillary pressure mercury injection quantification, and pore throat size distribution are all considered within this methodology (Jooybari et al. 2010). Thus, the reservoir volume can be divided into a few PRT with: (a) various bands of petrophysical properties, such as ϕ, k, water saturation, capillary pressure, or different connections between the fundamental assets; and (b) depositional facies and diagenesis are standard diagenetic features that determine the pore type, geometry, and petrophysical properties (Skalinski and Kenter 2015).

Conversely, log interpretation relies on various assessment procedures and is aligned with other methods. The combined results of these assessments reveal the presence of lithofacies or electrofacies, and it is expected that this will lead to similarities among the models proposed by different techniques. Reservoir classification is seen as a collaborative effort that involves reservoir engineering, petrophysics, and geology (Hollis et al. 2010).

In the literature, there are motivating works on the theme presented in the previous paragraph (Beiranvand et al. 2007; Al-Tooqi et al. 2014; Skalinski and Kenter 2015; Mehrabi et al. 2019). Beiranvand et al. (2007) identified reservoir rock types based on integrated data from core descriptions and petrographic analyses, mercury-injection capillary pressure, wireline logs, geophysical data, lithological, and pore-scale diagenetic history, which were then used to define the flow units and reservoir zones. The research contributed to a better understanding of flow unit distribution and reservoir modeling in this complex carbonate reservoir.

Al-Tooqi et al. (2014) used conventional core analyses, petrographic analysis, bulk chemistry, and mercury-injection capillary-pressure data to define PRTs. Skalinski and Kenter (2015) proposed a method for identifying and characterizing carbonate reservoirs by integrating geological attributes, petrophysical properties, and dynamic behavior. This approach aims to improve reservoir modeling by better understanding the influence of diagenetic processes and fractures on fluid flow.

Mehrabi et al. (2019) focused on classifying reservoir rock types and their distribution using a sequence-stratigraphic framework. It identifies different reservoir zones and rock types and interprets how these differences are related to the tectono-stratigraphic framework. The research also integrates data from cored intervals, electrofacies, and sequence stratigraphy to build a comprehensive reservoir model.

In terms of Brazilian reservoirs, those of the pre-salt layer are marked by complex carbonates exhibiting different kinds of ϕ and k. Research on this reservoir type has flow-unit segmentation strategies that primarily combine petrophysical techniques with rock types and geological classifications. This methodology aims to improve understanding of the connections between facies, diagenesis, and reservoir quality (Penna and Lupinacci 2020, 2021; Rebelo et al. 2022; Zeitoum et al. 2024; Rocha et al. 2025).

Classical hydraulic flow unit approaches remain among the most widely used techniques for improving permeability prediction in heterogeneous reservoirs because they integrate pore geometry, permeability, and connected porosity into a physically meaningful framework. Foundational studies by Amaefule et al. (1993) established the use of hydraulic flow units for uncored intervals, while more recent studies have demonstrated the applicability of FZI- and HFU-based workflows in carbonate reservoirs with strong heterogeneity and diagenetic overprint. For example, Khalid et al. (2020) showed that HFU methods improve reservoir zonation and permeability prediction, whereas Alizadeh et al. (2022) integrated FZI and well logs into artificial neural networks to improve permeability estimation in heterogeneous reservoirs.

More recently, machine learning approaches have become strategic tools for permeability prediction in carbonate systems. Studies by Al Khalifah et al. (2020), Xu et al. (2023), and Khalid et al. (2024) demonstrated that machine learning models can significantly improve permeability prediction by incorporating multiple logging responses and nonlinear relationships. In addition, physics-based machine learning approaches, such as the discrepancy modeling framework proposed by Akmal and Pyrcz (2025), have shown strong potential for integrating physical constraints with data-driven methods.

While integrated approaches have been successfully applied to the well-studied pre-salt reservoirs, their implementation in complex but distinct post-salt carbonate formations is less documented. These reservoirs exhibit intricate facies variations and diagenetic overprints that similarly defy simple porosity–permeability transforms (Carrasquilla and Silva 2019; Carrasquilla and Abreu 2023; Carrasquilla and Rocha 2025). Therefore, a critical question persists: Can a core-calibrated, flow-unit-based framework be effectively established and translated into a log-driven predictive model for post-salt carbonates?

This study answers this question by developing and validating a comprehensive workflow for the Linguado field. We demonstrate how systematically integrating core and log data to define Hydraulic Flow Units (HFUs) enables the derivation of unit-specific permeability transforms, achieving a step-change in prediction accuracy compared with conventional methods.

2 Geological background

Campos is one of the sedimentary basins delineated along the southeastern Brazilian continental shelf border, formed during the fragmentation of the supercontinent Gondwana. The tectonic adjustment of the plates during the Mesozoic era resulted in the fragmentation of extensive and largely stable continental blocks. In contrast, marine conditions dominated the basin during the Albian-Cenomanian period (Okubo et al. 2015). This research was performed on the Linguado oilfield within this basin, situated at 40° 50′ 00" west longitude and 22° 50′ 00" south latitude (Fig. 1).

Figure 2A illustrates the geological section of the Campos Basin, a typical Brazilian coastal basin. This figure illustrates this section's examined segment within a dashed red rectangle, specifically the post-salt layer's calcarenites. The salt layer is seen in purple in the illustration. Figure 2B presents an enlarged view of the section analyzed in the stratigraphic column of the Campos Basin, delineated by a dashed red rectangle in Fig. 2A (Okubo et al. 2015).

In this figure, the Macae Group consists of the Goitacas Formation, which includes the Quissama, Outeiro, Imbetiba, and Namorado Formations. The Quissama Formation (1) is an Albian carbonate reservoir in the lower section of the group, comprising clastic and oolitic carbonates that are locally fully dolomitized. The Outeiro Formation has calcilutite, marl, and shale of Albian age in its proximal section, whereas turbiditic sandstones from the Namorado Formation are present in its distal region. Subsequently, calcilutites from the Imbetiba Formation (4) in the proximal section of the Goitacas Formation, dating to the Cenomanian period, are presented. The turbiditic sandstone of the Namorado Formation (3) exists within the same geological age as the distal section of the Goitacas Formation, which

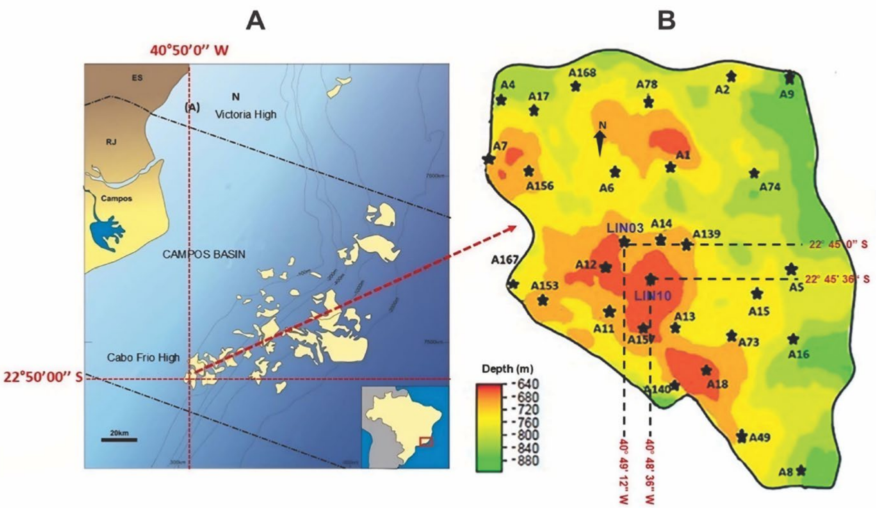

Fig. 1 Map of the location of the investigated oilfield in the southwest of the Campos Basin, with interception at longitude 40° 50′ 0″ west and latitude 22° 50′ 00″ south (**A**) and contour map of the basement depth (**B**), highlighting the locations of the Wells LIN03 and LIN10 (modified from Bruhn et al. 2003)

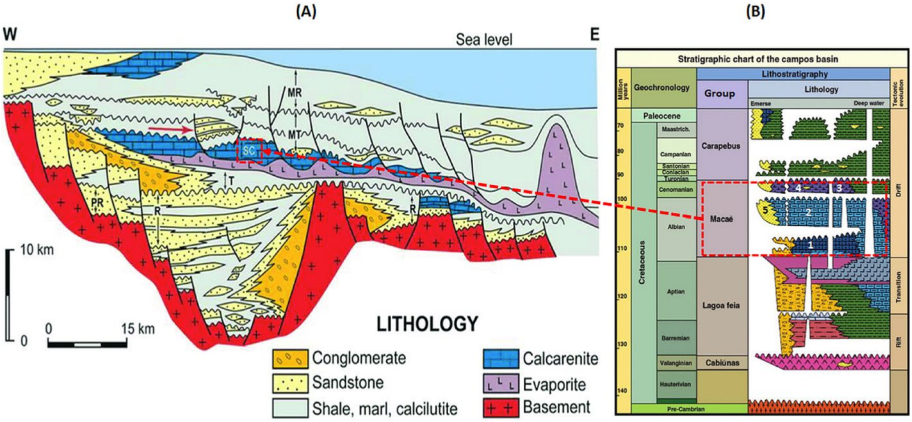

Fig. 2 **A** The general geologic section shows the basins along the eastern margin of Brazil. The four main mega sequences are PR (Pre-Rift), R (rift), T (Transitional, including the Evaporate Section), SC (Shallow Carbonate), MT (Marine Transgressive), and MR (Marine Regressive). **B** A closer look at the stratigraphy of the post-salt carbonates of the Campos Basin, focusing on the studied region, the dolomites and the calcarenites of the Quissama Formation (1), Outeiro Formation (2), Namorado Formation (3), Imbetiba Formation (4), and Goitacas Formation (5) (modified from Okubo et al. 2015)

comprises poorly sorted conglomerate and sandstone. The Namorado Formation, located in the distal part of the Goitacas Formation, is important to both the Outeiro and Imbetiba Formations. The Outeiro Formation contains Upper Albian turbidites, while the Imbetiba Formation comprises Middle to Upper Cenomanian turbidites (Formoso et al. 1991).

The Quissama Formation consists of grainstones and packstones composed of oncoids, ooids, peloids, and various bioclasts. These elements are connected to northern shoals formed in high to medium-energy environments. The Outeiro Formation is distinguished by fine carbonate strata alternating with marl and wackestone. This formation was produced due to a gradual rise in sea level that resulted in the submergence of the shallow carbonate platform of the Quissama Formation (Fig. 3). Moreover, these carbonate rocks are abundant in pelagic microfossils, such as calcispheres (notably pistonellids), planktonic foraminifera, and radiolarians (Okubo et al. 2015).

3 Materials and methods

The data from wells LIN03 and LIN10 of Linguado oilfield includes gamma-ray (GR), shallow (RXO), deep (RT) resistivities, bulk density (RHOB), neutron porosity (NPHI), and delay-time (DT) logs, together with ϕ and k laboratory data. The selected boreholes are approximately 700 m apart and possess a superior dataset compared to the other 25 wells of the oilfield. The laboratory ϕ was measured with the helium porosimeter in core samples, representing the effective porosity (ϕ_e) as it pertains to the interconnected pore spaces accessible to the gas. The permeability was measured in the laboratory by flowing helium through a sample and measuring the flow rate or pressure drop (Petrobras 2012; ANP 2019). These data were initially interpreted using the Interactive Petrophysics (IP) software

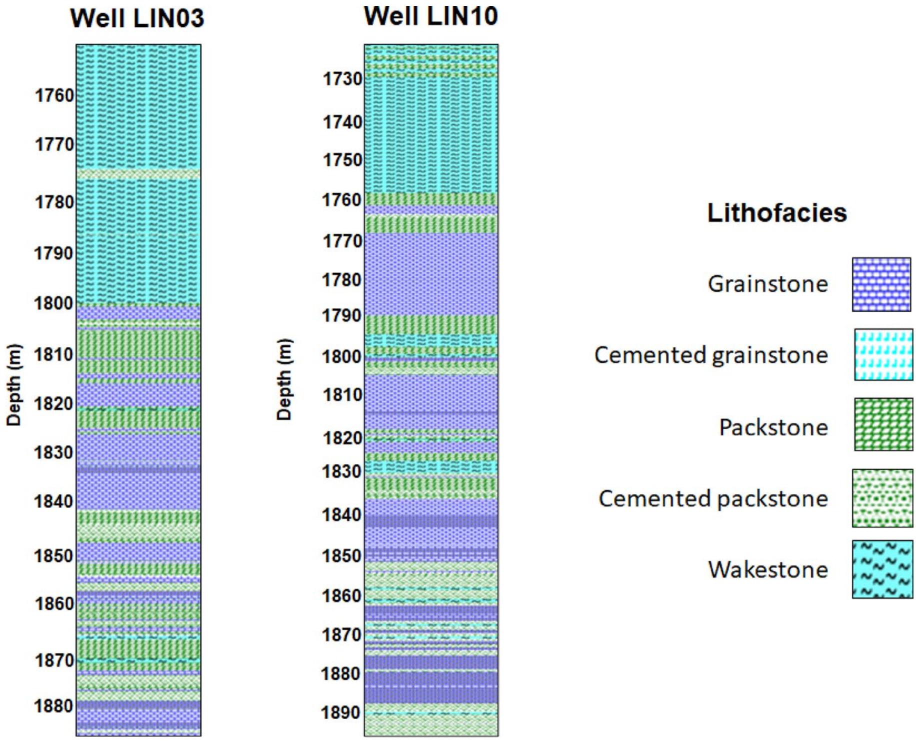

Fig. 3 Lithofaces of wells LIN03 (left) and LIN10 (right) located in Fig. 1b (modified from Okubo et al. 2015)

(Geoactive 2023), and calculations and visualizations were also conducted using the MATLAB platform (MATLAB 2021).

Many empirical relationships relate ϕ and k, among them the Timur approach (Timur 1968), which is one of the best-known models for predicting k, derived using the equation:

$$k^a = b\left(\frac{\phi_e^c}{S_{WIRR}}\right), \quad (1)$$

where k is the permeability (mD), a = 0.5, b = 93, and c = 2.2 are regression constants, ϕ_e is the effective porosity (%), and S_{WIRR} (%) is the irreducible water saturation. The DT log measures the acoustic transit time in the formation, and DT porosity (ϕ_{DT}) obtained from this log is expressed by:

$$\phi_{DT} = \frac{\Delta t_{LOG} - \Delta t_{MAT}}{\Delta t_{FLU} - \Delta t_{MAT}}, \quad (2)$$

where ϕ_{DT} is the travel time porosity (µs/feet), Δt_{LOG} is the measured interval travel-time (µs/feet), Δt_{MAT} is in the rock matrix (µs/feet), and Δt_{FLU} is in the saturating fluid (µs/feet). As it is a carbonate reservoir, Δt_{MAT} = 45 µs/feet for limestone and Δt_{FLU} = 230 µs/feet for oil from the oil zone. As ϕ_{DT} indeed measures primary porosity, and it was used to asses the values that most closely align with ϕ_e, the laboratory measurements (Nugent 1984).

On the other hand, k, ϕ, and the capillary pressure parameters are related by the Winland–Pittman method. This empirical equation has demonstrated efficacy as a cut-off criterion for finding commercial hydrocarbon reserves in stratigraphic traps (Winland 1972). The regression equation derived from laboratory data is:

$$r_{35} = 5.40\left(\frac{k^{0.59}}{\phi^{0.86}}\right), \tag{3}$$

where r_{35} represents the predicted pore throat radius (μm) at 35% mercury saturation during the injection capillary pressure test, k denotes the permeability (mD), and ϕ signifies porosity (%) (Aguilera 2002). This equation can predict comparable r_{35} values for core samples of a specific petrophysical rock type (PRT) or flow unit (FU) in wells lacking capillary pressure data. This equation can be simplified in the form:

$$r_{35} = 2.67\left(\frac{k}{\phi}\right), \tag{4}$$

which calculates the pore-throat radius at 35% mercury saturation, with k measured in mD and ϕ expressed as a percentage (Omeje et al. 2022).

The stratigraphic modified Lorenz plot (SMLP) technique was subsequently employed to examine the dataset. The SMLP method is a laboratory-generated cross-plot of ϕ and k derived from core data. This strategy is a highly effective FU discriminating technique grounded in geological structure, cumulative storage capacity (ϕ_h, %), and cumulative flow capacity (k_h, %). k_h represents the product of k and h (thickness, m), whereas ϕ_h denotes the product of ϕ and h (%). The formulae:

$$k_h = \left(\left[\frac{k_1(h_1 - h_0) + k_2(h_2 - h_1) + \ldots k_i(h_i - h_{i-1})}{\sum k_i(h_i - h_{i-1})}\right]\right), \tag{5}$$

and

$$\phi_h = \left(\left[\frac{\phi_1(h_1 - h_0) + \phi_2(h_2 - h_1) + \ldots \phi_i(h_i - h_{i-1})}{\sum \phi_i(h_i - h_{i-1})}\right]\right), \tag{6}$$

delineate the mathematical expressions employed for their computation, where k_i, ϕ_i, and h_i represent the permeability (mD), porosity (%), and thickness (m) of the respective layers. k_h and ϕ_h represents the cumulative flow and storage capacity (Tiab and Donaldson 2015).

The reservoir quality index (RQI), flow zone indicators (FZI), and the Winland–Pittman approach were employed to allocate the FU across the reservoir (Pittman 1992). The equation

$$RQI = 0.0314\left(\frac{k}{\phi}\right), \tag{7}$$

was used to calculate the RQI, where k represents the permeability (mD), and ϕ is the sonic porosity (%), which is the connected porosity (Amaefule et al. 1993). FZI is a function of RQI, expressed as:

$$\mathrm{FZI} = \frac{\mathrm{RQI}}{\phi_z}, \tag{8}$$

where ϕ_z is the pore volume to grain volume fraction, defined as:

$$\phi_z = \frac{\phi}{1 - \phi}. \tag{9}$$

Each straight line signifies analogous pore throats, and an FU is identified based on FZI in the cross-plot between ϕ_z and RQI on a log–log scale. PRT constitutes the geological framework, whereas ϕ_h is the basis for the graphical technique to estimate reservoir FU (Gunter et al. 1997).

Samples exhibiting different FZI values are organized in supplementary parallel lines, illustrating a characteristic hydraulic flow unit (HFU) and analogous pore throat properties. The mean FZI value most accurately reflects the characteristics of each zone with a minimal margin of error. HFUs are computed utilizing the parameters k and ϕ as inputs in conjunction with the PRT concept. Consequently, the HFU is calculated using the RQI in conjunction with ϕ_Z cross-plot when the value of $\phi_Z = 1$ is plotted on a logarithmic scale. Low HFU values result from rocks characterized by poorly sorted, fine grains with a substantial surface area and elevated tortuosity. Conversely, elevated HFU values result from rocks characterized by well-sorted, coarse grains with a reduced surface area and a diminished formation factor and tortuosity (Dunham 1962).

The equations for k in each HFU are solved using a linear regression (Amaefule et al. 1993):

$$\mathrm{k} = \frac{\left(\mathrm{FZI}^2 \phi^3\right)}{\left(0.031\,(1 - \phi)\right)^2}, \tag{10}$$

where k, FZI, and ϕ_e are as defined above.

The central philosophy of our methodology is to use detailed core data from key wells to uncover the reservoir's underlying hydraulic structure. This geological–petrophysical framework is then used to train the response of conventional geophysical logging. The subsequent steps, detailed below, follow this progression from core-scale analysis to logging-scale application.

This logical progression is summarized in the workflow diagram (Fig. 4), where the dynamic parameters for the reference well LIN03 were assessed and subsequently applied to the blind test well LIN10, utilizing the existing correlation between the two boreholes. In summary, this work adopts the following order for the determination of permeability: Winland–Pittman method, SMPL, RQI, FZI, and HFU, and the sequence culminates in a linear regression to estimate the permeability in each HFU in the post-salt reservoir in southeastern Brazil, which becomes the innovation of the estimate (Lichotti 2016).

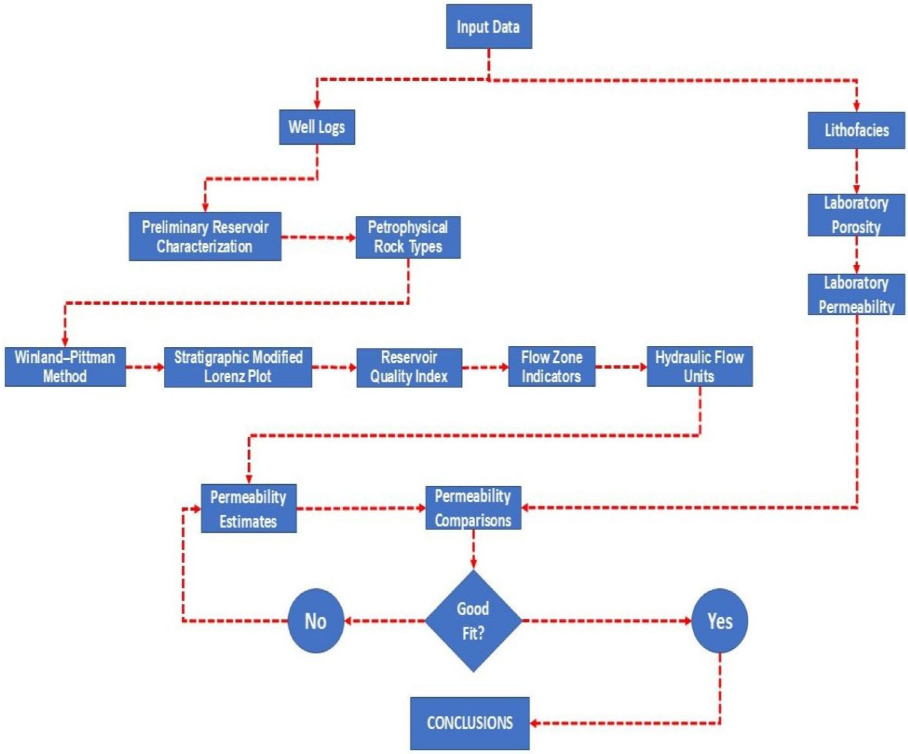

Fig. 4 All steps of the workflow followed in this study (Lichotti 2016)

4 Results and discussions

The application of our integrated workflow produced a transformative improvement in permeability estimation. Moving from a generic empirical model (Timur equation, $R^2=0.12$) to specific HFU models increased the coefficient of determination to $R^2>0.97$, effectively bridging the gap between well-log predictions and core measurements. The following sections detail the steps that led to this result.

The log data for the wells LIN03 (Fig. 5A) and LIN10 (Fig. 5B) are organized into tracks: (1) depth (m); (2) *te*mperature (°F); (3) fluids; (4) GR (°API) log; (5); NPHI (%, blue) and RHOB (r/cm^3, red) logs; (6) DT (μs/feet) log; (7) *s*hallow RXO (pink) and deep RT (red) resistivity logs (Ω m). Data for LIN03 is between 1750 and 1890 m in depth, with potential reservoir rocks located between 1800 and 1890 m. For LIN10, the data range from 1720 to 1900 m in depth, with prospective reservoir rocks identified between 1770 and 1890 m.

The qualitative comparison of the log data indicates that the rocks possess similar geological properties, with correlations between the electrofacies of the two wells evident in the GR (track 4) and DT (track 6) logs. The GR log indicates elevated values in both wells at shallow depths (50 and 100 ºAPI), suggesting the presence of finer-grained, more argillaceous carbonate facies, such as wackestones, mudstones, or marly intervals. However, this interpretation should not rely exclusively on GR response, since high GR values in carbon-

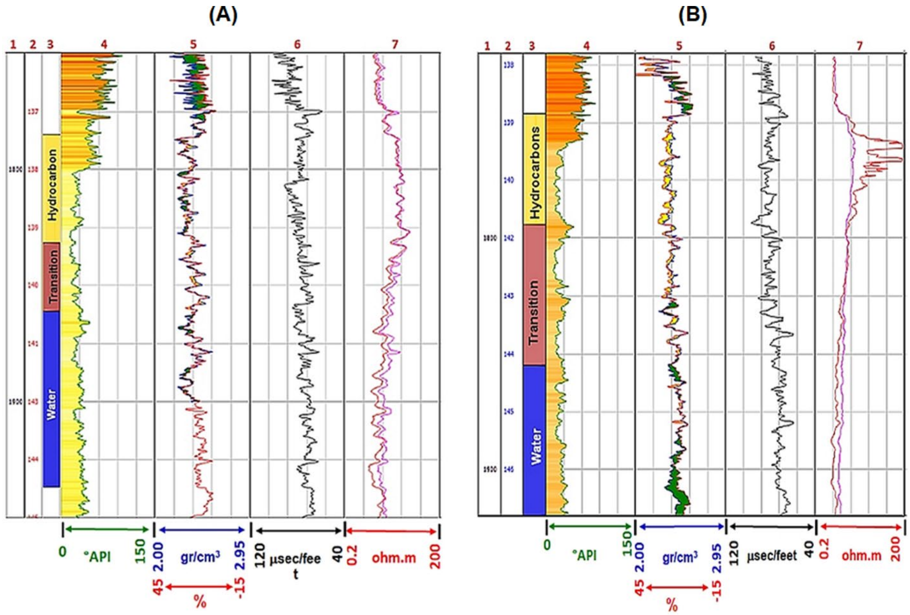

Fig. 5 **A** Wells LIN03 (blind test) and **B** LIN10 (reference). Tracks: (1) depth (m); (2) temperature (°F); (3) fluids; (4); GR (°API) log; (5) NPHI (%, blue) and RHOB (g/cm^3, red) logs; (6) DT log (μs/feet); (7) shallow RXO (pink) and deep RT (red) resistivity logs (Ω m) (Petrobras 2012; ANP 2019)

ate reservoirs may also reflect shale content, stylolites, uranium enrichment, or dolomitization. Therefore, the interpretation of wackestone was supported by lithological descriptions, core information, and the associated petrophysical behavior. GR measurements fall below 40 ºAPI at intermediate and deep levels, indicating a zone with low wackestone composition, which is essential for optimal reservoir rock quality. The DT log indicates elevated values (70 and 100 us/ft) at shallow depths, explaining why wackestone results in long transit durations that align with the variations observed in the GR log. At intermediate and deep depths, the DT log exhibits significant oscillations, with values ranging from 60 to 100 us/ft, a phenomenon commonly observed in carbonate reservoirs due to the variability of these rocks.

The RHOB and NPHI logs (track 5) converge at intermediate depths, with RHOB on the left and NPHI on the right; this convergence is generally associated with hydrocarbon accumulations (indicated by yellow shading). The green shading signifies the presence of water, with RHOB on the right and NPHI on the left. The curves sometimes reverse at significant depths, corroborating the existence of a probable transition zone and a potential water zone at higher depths, as indicated by the resistivity data analysis. The RT and RXO logs (track 7) show values below 20 Ω m in the pink-shaded area at shallow depths, indicating their presence in non-reservoir zones. At intermediate depths, the value rises to approximately 200 Ω m, indicating hydrocarbon accumulation. Both resistivity curves exhibit lower values with increasing depth, indicating a transition zone that stabilizes at approximately 4 Ω m, corresponding to a water zone. The overlap and subsequent separation of these two resistivities upon entry of drilling mud indicate the permo-porous characteristics of the formation being examined. RT resistivity exceeds RXO at depths containing hydrocarbons and is lower in regions with water, according to Da Costa et al. (2019).

The comparison of porosity derived from logs with core porosity served as a critical quality check and selection process. Although all correlations showed dispersion inherent to heterogeneous carbonates, the porosity derived from sonic flow (ϕ_{DT}) matched the effective core porosity most closely (Fig. 6). This confirmed its suitability as the main input parameter for subsequent permeability modeling, as it more closely reflects the interconnected pore network relevant to fluid flow.

The NPHI log was directly measured ϕ, while it was indirectly estimated using the DT (ϕ_{DT}) and RHOB (ϕ_{RHOB}) logs. The comparison of these estimates with the laboratory data produced R2 values of 29.08% and 51.20%, 20.82% and 50.31%, and 13.87% and 37.01% for the ϕ_{DT}, ϕ_{RHOB}, and ϕ_{NPHI} across both wells, respectively (Fig. 6). As ϕ_{DT} measures primary porosity and was used to identify the values that most closely align with ϕ_e, the laboratory measurements. Consequently, the ϕ estimate derived from the DT log is slightly superior to other alternatives and was chosen for the subsequent calculations.

Figure 7A illustrates the r_{35} curves of the Winland–Pittman method for LIN03, whereas Fig. 7B presents those for LIN10, described through a crossplot of ϕ vs. k. The red curves depicted collectively correspond to the pore necks' respective values (r_{35}). The delineations of the individual point clusters were determined using k-means clustering in the IP program (Geoactive 2023).

The clusters identified through k-means analysis should not be interpreted as definitive depositional lithofacies classifications. Instead, they represent petrophysical groupings defined by similarities in porosity, permeability, pore-throat radius, reservoir quality index, flow zone indicator, and hydraulic flow unit behavior. The lithological affinity of each cluster is therefore inferred from the associated petrophysical characteristics and the regional geological framework for the studied interval. Consequently, the clusters are more appro-

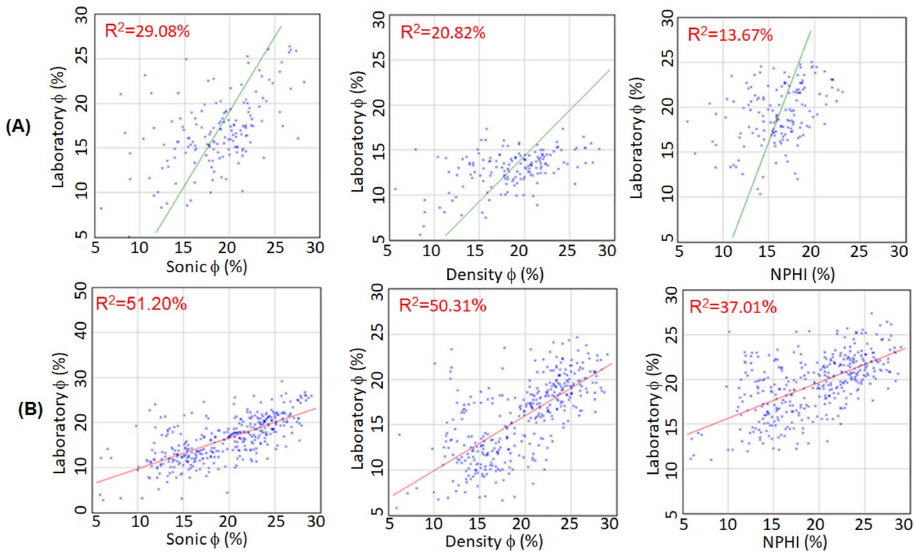

Fig. 6 Comparison between laboratory ϕ and estimated ϕ with sonic, density and neutronic logs for wells **A** LIN03 and **B** LIN10

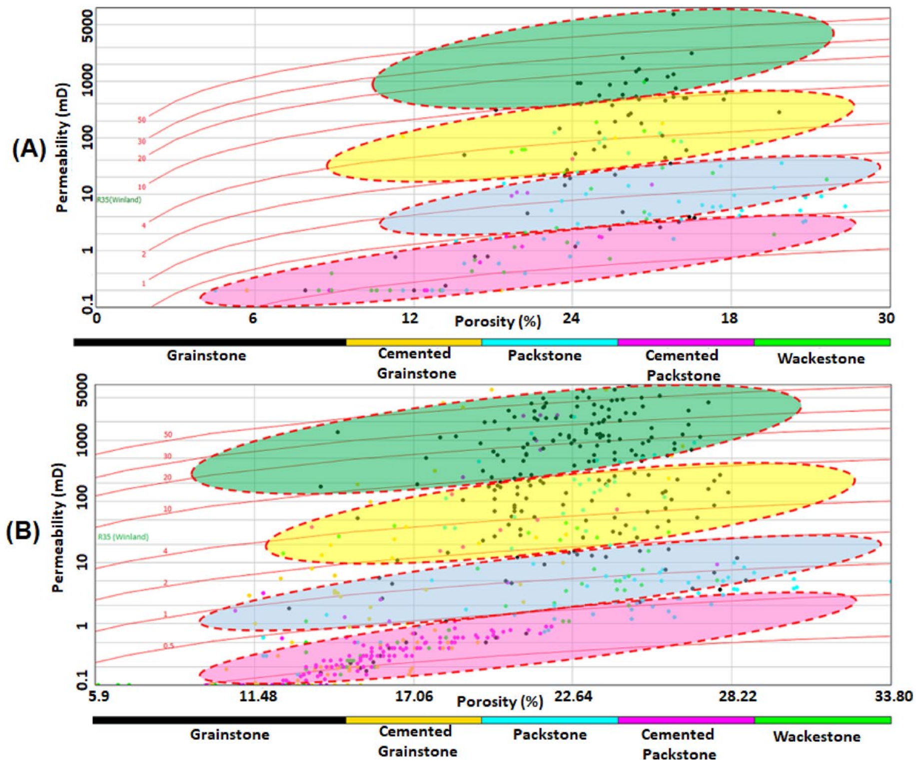

Fig. 7 Distribution of pore sizes with Winland (1972) R35 curves for wells LIN03 (**A**) and LIN10 (**B**): green (≥ 10 µm), yellow (2–10 µm), blue (0.5–2 µm), and pink (< 0.5 µm), corresponding to, respectively, mega (grainstones), macro (not cemented grainstones and packstones), meso (cemented packstones, wackstones, and few grainstones) and micro (packstones, cemented packstones and wackstones) pores

priately described as petrophysical facies or hydraulic classes with probable correspondence to grainstones, packstones, wackestones, or cemented intervals, rather than as strictly validated lithofacies.

In examining group 1 (green), characterized by mega-pores of 10 mm, cemented grains are predominant. The macro-pores of group 2 (yellow) vary from 2 to 10 mm. Specific locations within this group can be associated with packstones and uncemented grainstones. Meso-pores ranging from 0.5 to 2 mm are in group 3 (light blue). This group's lithology mainly consists of packstones, cemented packstones, wackestones, and grainstones. Finally, group 4 (pink) contains micro-pores with a pore size under 0.5 mm and a more significant proportion of points associated with packstones, cemented packstones, and wackestones.

The Winland–Pittman analysis proved particularly useful for distinguishing pore-system classes with different hydraulic behaviors. The identified mega-, macro-, meso-, and micro-pore groups reflect variations in pore-throat radius, permeability, and connectivity, allowing differentiation between intervals with high flow capacity and tighter reservoir zones. Therefore, the pore-throat classes are not only descriptive categories, but also important indicators of reservoir quality and fluid-flow efficiency.

The most productive intervals correspond to the flow units associated with larger pore-throat radii and better pore connectivity, particularly the mega- and macropore groups identified by the Winland–Pittman method. These intervals are generally related to grainstones, uncemented grainstones, and packstones with lower tortuosity and higher permeability. In contrast, intervals dominated by meso- and micropores, commonly associated with cemented packstones and wackestones, tend to show poorer reservoir quality due to smaller pore throats and lower connectivity.

For the FU analysis, laboratory measurements of ϕ and k from drill cores were used for LIN03, yielding the SMLP cross-diagram of ϕ_h vs. k_h along the borehole in the reservoir region. The quantity of FU was ascertained at the inflection points shown on the curves. The signify changes in slope in the diagram, indicating fluctuations in the flow characteristics of the porous medium. The initiation of an FU and the conclusion of a preceding FU are defined by the presence of inflection points (red dots). Horizontal lines, typically flat, signify impediments to the movement. The curves' nearly 45°-sloped segments show the FU's substantial flow capacity, as indicated by the green arrows between the red inflection points. This approach exemplifies the challenges that may arise while delineating FU. In LIN03, seven inflection sites are observed on the curve, determining eight FUs (Fig. 8A). Figure 8B illustrates the same technique employed for LIN10. Following the SMLP methodology, the FU number for both wells was set to 8.

The flatter segments of the SMLP curves are interpreted as flow barriers or low-flow zones, generally associated with wackestones, cemented packstones, and intervals dominated by meso- and micropores. In contrast, the steeper segments of the curves represent preferential flow channels, commonly related to grainstones, uncemented packstones, and intervals with mega- and macropores, where permeability and pore connectivity are higher.

The hydraulic flow units identified in this study should not be interpreted as strictly continuous layers distributed uniformly throughout the reservoir. Instead, they represent recurring hydraulic classes defined by similar porosity, permeability, pore-throat radius, and flow behavior. Although local heterogeneity may produce discontinuous HFU occurrences along the reservoir profile, the vertical recurrence of similar petrophysical signatures suggests that some hydraulic classes can be recognized repeatedly where comparable depositional facies and diagenetic conditions are present. Therefore, the HFUs were used as representative flow-related groupings rather than as laterally continuous stratigraphic bodies.

The HFU values for the samples vary from 0.14 to 21.17 for LIN03 (Table 1) and from 0.071 to 259.67 for LIN10 (Table 2). For each FU, the k equations were derived by linear

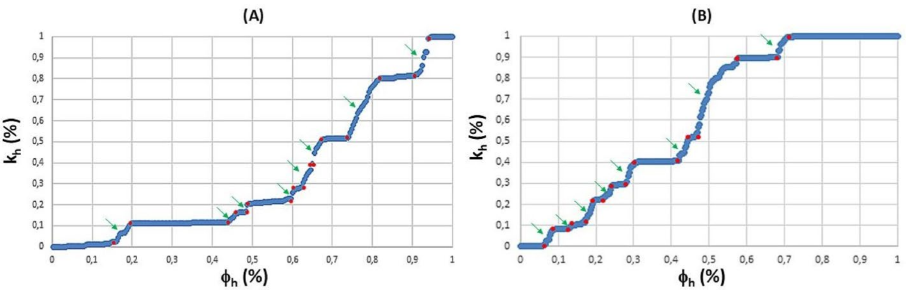

Fig. 8 Stratigraphic modified Lorenz plot (SMLP) for wells LIN03 (**A**) and LIN10 (**B**), with red dots indicating the inflection points of the curves and green arrows for the flow units

Table 1 Hydraulic flow units, ranges of corresponding flow zone indexes, equations for permeability based on sonic log porosity of well LIN03

HFU	FZI ranges	Permeability equations	R^2 (%)
1	0.14–0.25	$k = \phi^3(0.14/(0.031(1-\phi)))^2$	92.59
2	0.25–0.38	$k = \phi^3(0.31/(0.031(1-\phi)))^2$	96.51
3	0.38–0.53	$k = \phi^3(0.43/(0.031(1-\phi)))^2$	98.68
4	0.53–0.87	$k = \phi^3(0.71/(0.031(1-\phi)))^2$	97.92
5	0.87–1.49	$k = \phi^3(1.10/(0.031(1-\phi)))^2$	95.32
6	1.49–3.08	$k = \phi^3(2.14/(0.031(1-\phi)))^2$	34.05
7	3.08–6.65	$k = \phi^3(4.54/(0.031(1-\phi)))^2$	35.87
8	6.65–21.17	$k = \phi^3(9.20/(0.031(1-\phi)))^2$	35.18

Table 2 Hydraulic flow units, ranges of corresponding flow zone indexes, equations for permeability based on sonic log porosity of well LIN10

HFU	FZI ranges	Permeability equations	R^2 (%)
1	0.071–0.25	$k = \phi^3(0.19/(0.031(1-\phi)))^2$	92.59
2	0.25–0.38	$k = \phi^3(0.31/(0.031(1-\phi)))^2$	96.51
3	0.38–0.67	$k = \phi^3(0.48/(0.031(1-\phi)))^2$	98.68
4	0.67–2.14	$k = \phi^3(1.23/(0.031(1-\phi)))^2$	97.92
5	2.14–4.78	$k = \phi^3(3.23/(0.031(1-\phi)))^2$	95.32
6	4.78–7.89	$k = \phi^3(6.06/(0.031(1-\phi)))^2$	34.05
7	7.89–18.00	$k = \phi^3(11.86/(0.031(1-\phi)))^2$	35.87
8	18.00–259.68	$k = \phi^3(22.82/(0.031(1-\phi)))^2$	35.18

regression, and R^2 indicates the goodness of fit for LIN03 (Table 1) and LIN10 (Table 2). For LIN03, the values exceed 80% for the initial five HFUs and fall below 80% for the remaining three.

Conversely, for LIN10, these values exceed 90% for the initial five HFUs and fall below 90% for the next three. The data with corresponding FZI values were categorized into the same HFU according to the parameters established by the cluster analysis. This process was executed to enhance the representation of the HFU in the reservoir. On the contrary, these images illustrate the ϕ_z vs. RQI crossplots, in which the HFUs and clusters are distinctly represented in eight different colors for LIN03 (Fig. 9) and LIN10 (Fig. 10).

The successful grouping of data into distinct HFUs in the FZI-ϕ_z plot (Figs. 9 and 10) validates the existence of discrete petrophysical populations within the reservoir, each with a unique pore bottleneck architecture. The high R^2 values of the permeability equations for the lower FZI units (Tables 1 and 2) indicate that these zones are internally consistent. The lower R^2 in the higher FZI units likely reflects their more vugular or fractured nature, where permeability becomes less controlled solely by interparticle porosity, a crucial insight for reservoir modeling.

Figure 11 shows the correlation between the k estimated using ϕ_{DT} and the laboratory k for wells (A) LIN03 (R^2=88.55%) and (B) LIN10 (R^2=96.39%). The k estimate by the RQI method was calculated utilizing the laboratory (track 6) and DT (track 7) porosities for

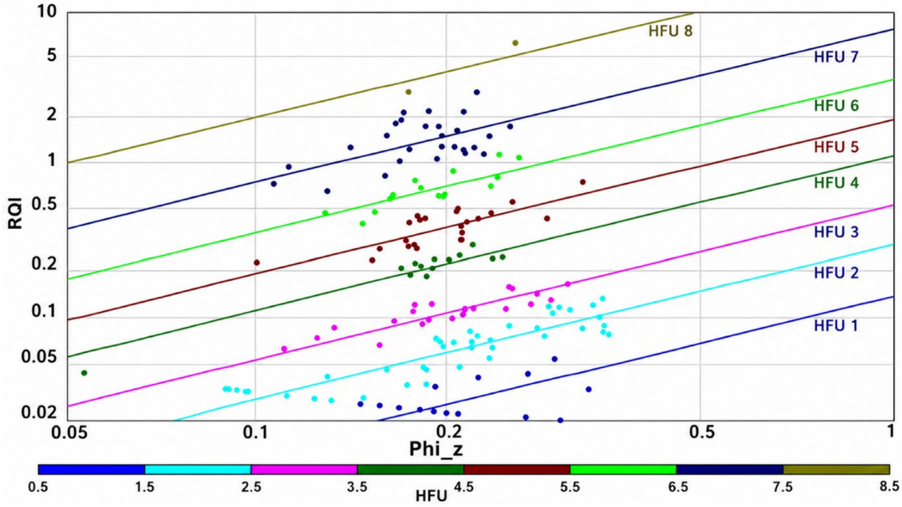

Fig. 9 Pore volume to grain volume fraction (ϕ_z) versus reservoir quality index (RQI), calculated with sonic log porosity for well LIN03

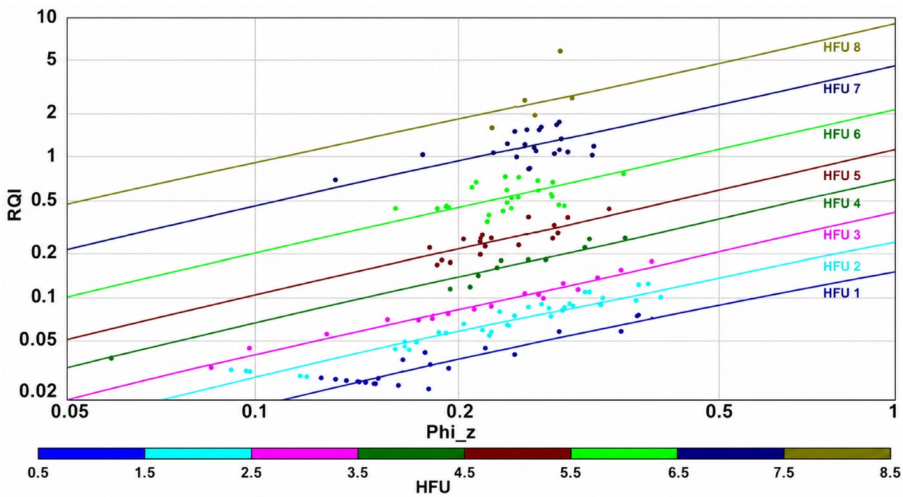

Fig. 10 Pore volume to grain volume fraction (ϕ_z) versus reservoir quality index (RQI), calculated with sonic porosity for well LIN10

LIN03 (Fig. 12) and LIN10 (Fig. 13). The data illustrate the lithofacies in track 2, the SMLP curve in track 3, the FZ in track 4, the FU in track 5, and the k-estimates in tracks 6 and 7.

In both figures, the black dots represent the k values obtained from laboratory measurements on plugs. The k-curve is a compound of the regression curves for each HFU. The concordance between the estimates and the laboratory results indicates that the models are coherent. The coefficient of determination R^2 is 0.90 for LIN03 and 0.89 for LIN10 when utilizing laboratory ϕ (track 6 in both figures). Utilizing ϕ_{DT} yields $R^2=0.97$ for LIN03 and

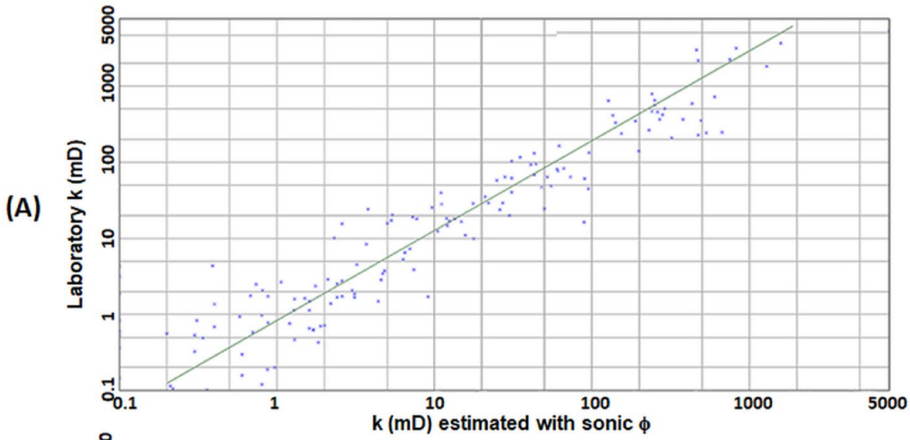

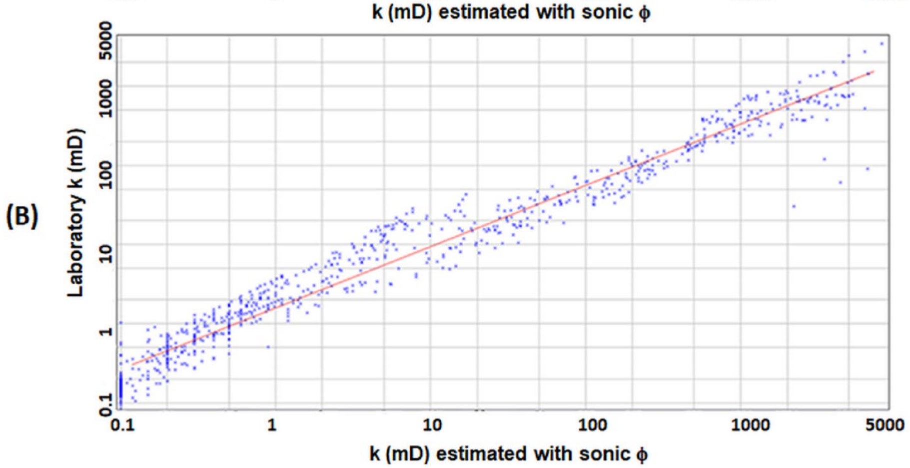

Fig. 11 Correlation between the permeability estimated using the sonic k and the laboratory k for wells LIN03 (**A**) and LIN10 (**B**)

$R^2 = 0.98$ for LIN10 (track 7 in both figures). The correlation between the k-peaks in red (track 6) and pink (track 7) and the black FU curve (track 5) is observable. Consequently, the k model generated from the FU equations is reliable in both wells.

The two boreholes were analyzed to identify ways to correlate the zones identified in both wells and to better understand the carbonate reservoir. The eight FUs identified for each well were primarily analyzed in the reservoir zone, which had similar patterns (Fig. 14, track 4). The similarities between the traditional logs were examined in a second step. The GR, RHOB, NPHI, and DT logs showed the same behavior in both wells studied, confirming the previously observed correlations between the FUs (Fig. 15, tracks 2–4).

Although the methodology showed strong agreement between LIN03 and LIN10, the present validation remains local in scale and should not be interpreted as definitive proof of field-wide transferability. The two wells are separated by approximately 700 m and exhibit similar geological and petrophysical characteristics, supporting the reproducibility of the workflow under comparable reservoir conditions. However, additional wells distributed across the field's different structural and depositional domains would be necessary to evalu-

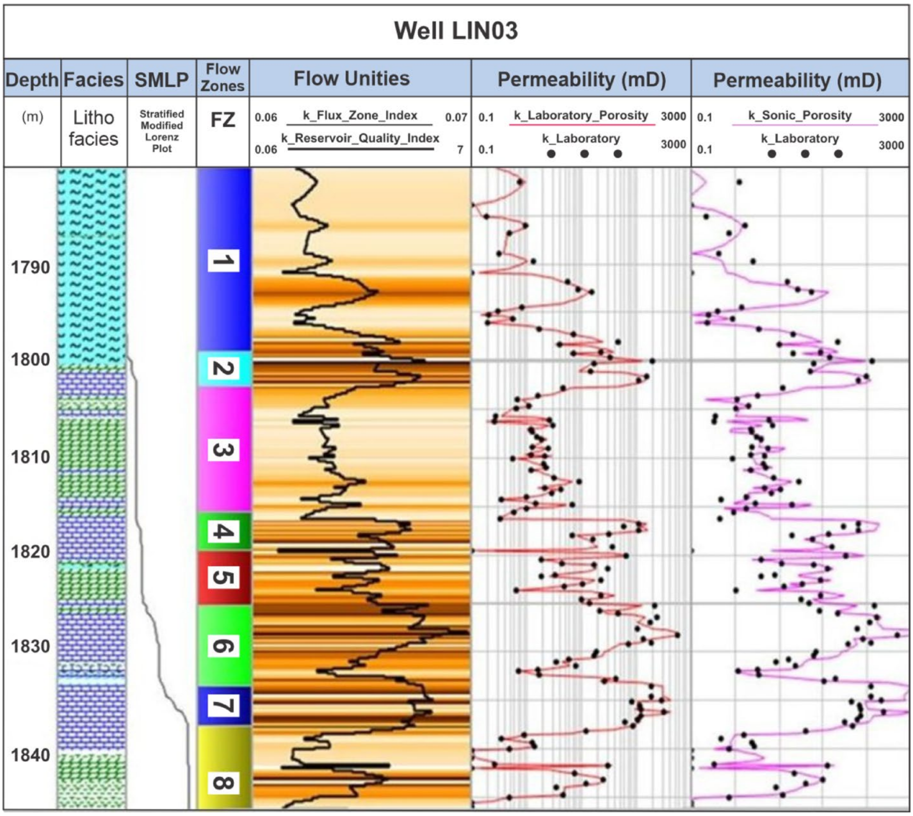

Fig. 12 Tracks for well LIN03: (1) depth (m); (2) lithofacies; (3) Stratified modified Lorenz curve; (4) flow zones; (5) flow unities, flow zone index is plotted as shading and reservoir quality index as the black curve; (6) the red curve is the permeability estimate (mD) using laboratory porosity, and the black dots are the laboratory permeability. (7) The pink curve is the permeability estimate (mD) using sonic log porosity, and the black dots are the laboratory permeability

ate the lateral continuity of the hydraulic flow units and the broader applicability of the permeability transforms.

5 Conclusions

This study utilized geophysical well logs and petrophysical laboratory data from two boreholes to assess the permeability of a carbonate reservoir in the Linguado oilfield, located in the Campos Basin, southeastern Brazil. The research aimed to address the challenges in the evaluation and was motivated by the notable variation in carbonate rocks. Porosity was first determined using various logs, and the results were compared with those obtained from laboratory testing. The neutron porosities (0.14 and 0.37) and density porosities (0.21 and 0.50) had the lowest Pearson's coefficient of determination (R^2) in wells LIN03 and LIN10. The sonic log gave better results (0.29 and 0.51), and therefore, it was employed to evaluate all permeabilities.

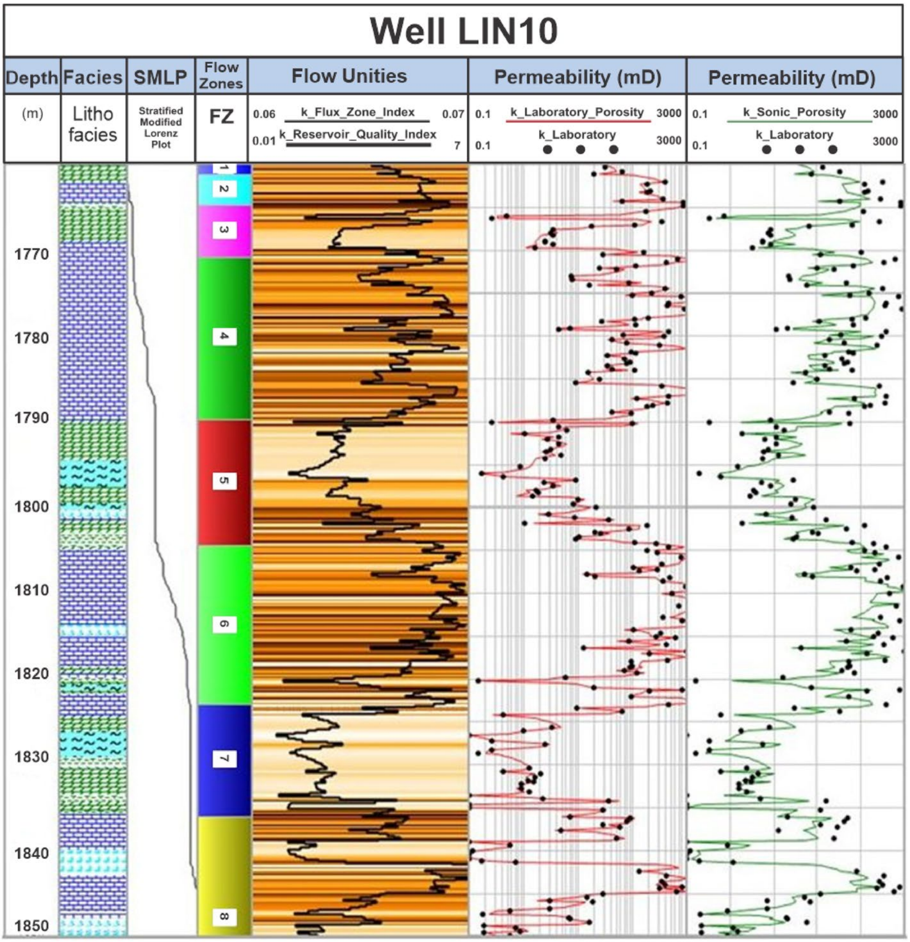

Fig. 13 Tracks for well LIN03: (1) depth (m); (2) lithofacies; (3) Stratified modified Lorenz curve; (4) flow zones; (5) flow unities, flow zone index is plotted as shading and reservoir quality index as the black curve; (6) the red curve is the permeability estimate (mD) using laboratory porosity, and the black dots are the laboratory permeability (mD). (7) The green curve is the permeability estimate (mD) using sonic log porosity, and the black dots are the laboratory permeability (mD)

The Timur assessment had an R^2 of 0.12, indicating the need for more reliable models that, for example, divide the reservoir into zones based on lithofacies, flow zones, and hydrodynamic flow units. This grouping yielded regression equations for each hydrodynamic flow unit, demonstrating the approach's effectiveness. Combining the different equations into a single expression, we obtained $R^2 = 0.97$ for LIN03 and $R^2 = 0.98$ for LIN10, based on the reservoir quality index.

Eight flow units were identified in both LIN03 and LIN10, indicating that the reservoir can be subdivided into recurring hydraulic classes with similar petrophysical behavior. The correspondence of these flow units between the two wells suggests that the same hydraulic architecture may be recognized under comparable geological conditions. However, these flow units should not be interpreted as strictly continuous layers throughout the entire field,

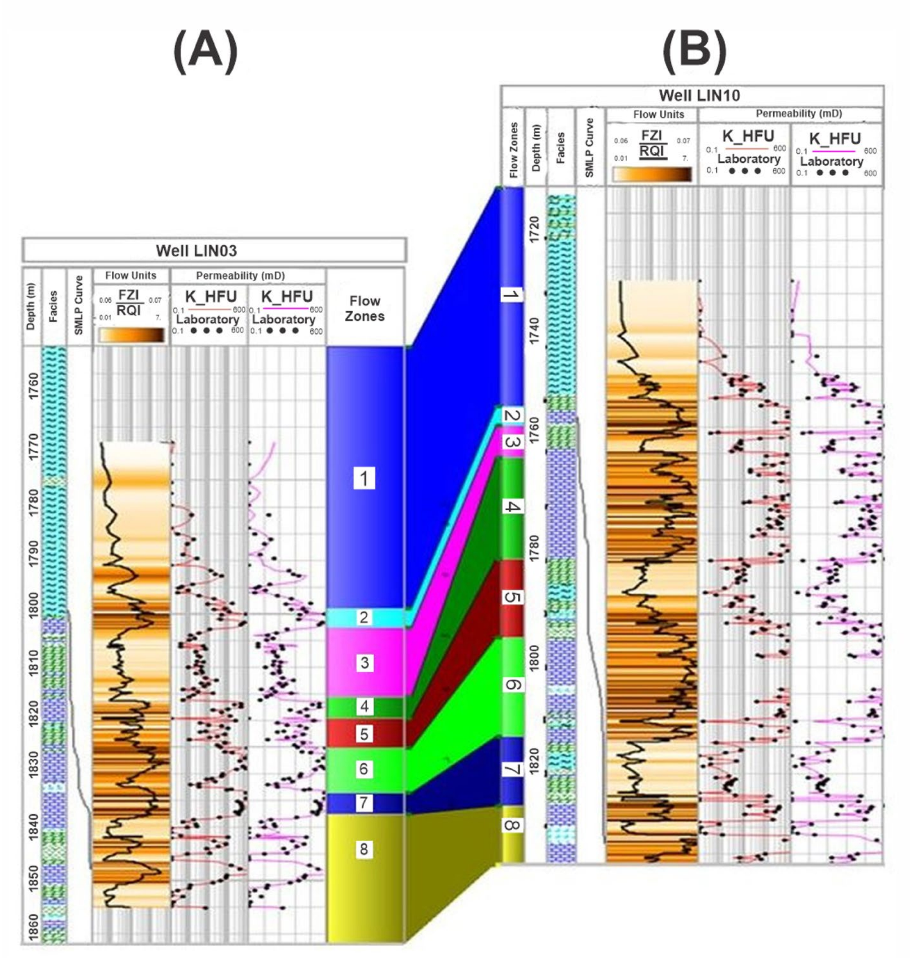

Fig. 14 Comparing petrophysical results for wells: **A** LIN03 and **B** LIN10: (1) depth (m); (2) lithofacies; (3) Stratified modified Lorenz curve; (4) flow unities, flow zone index is plotted as shading and reservoir quality index as the black curve; (5) the red curve is the permeability estimate (mD) using laboratory porosity, and (6) the black dots are the laboratory permeability (mD). (7) The pink curve is the permeability estimate (mD) using sonic log porosity, and the black dots are the laboratory permeability (mD); flow zones

since local variations in facies, diagenesis, and structural position may affect their vertical and lateral distribution.

From this result, the flow zones and units in both wells could be identified, allowing LIN10 to be effectively used as a blind test. The productive zones in both wells exhibit mega- and macropores, attributable to lithofacies with uncemented grains, indicating favorable permeoporous characteristics consistent with the reservoir quality index study. The wells are 700 m apart and vertically offset by 30 m, suggesting that wellbore placement on the structural height of the carbonate ramp influences each borehole's reservoir quality and productivity. This study concludes that integrating petrophysical and geological data

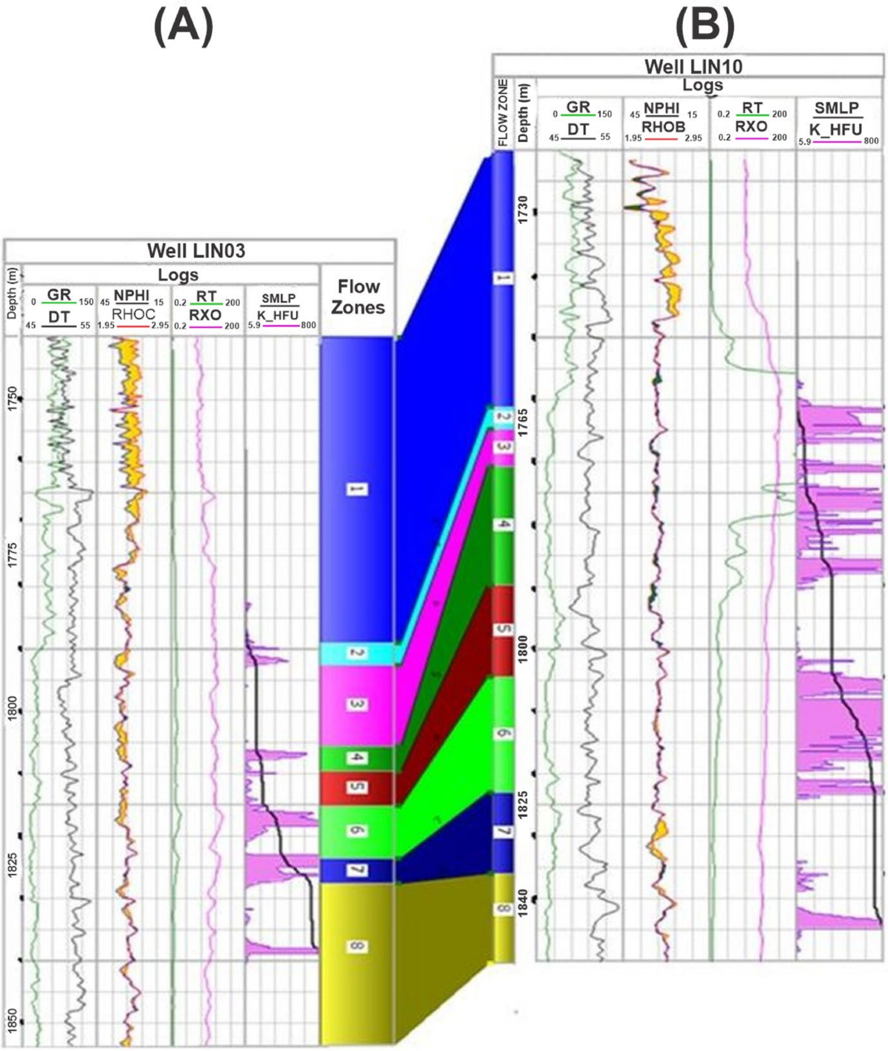

Fig. 15 Comparing basic logs for wells: **A** LIN03 and **B** LIN10: (1) depth (m); (2) GR (°API) and DT (μs/feet); (3); NPHI (%) and RHOC (g/cm^3) (4) RXO and RT (Ω m); (5) SMLP and k_{HFU}; and (6) flow zones

enhances the inference of reservoir characteristics, enabling their application and extrapolation to other wells in the studied oilfield.

This study culminates in more than just an improved permeability curve for two wells. It provides a transferable framework for characterizing heterogeneous carbonate reservoirs. By rigorously integrating geological (flow units) and petrophysical (core-well log) data, we move from descriptive rock typification to predictive modeling of hydraulic units.

The workflow demonstrates that the key to accurate permeability prediction lies not in seeking a universal transformation, but in using core data to decode the reservoir's hydraulic architecture and then calibrating well log responses to it. This approach significantly reduces risk in evaluating non-core intervals and new wells in the Linguado field and offers a validated strategy for analogous post-salt carbonate reservoirs worldwide.

Acknowledgements The authors express gratitude to the Brazilian National Research Agency (CNPq) for the research grant, the Petroleum Engineering and Exploration Laboratory (UENF/LENEP) for the computational infrastructure, the National Institute of Geophysical Science and Technology (INCT-GP) for its support, and ANP (Brazilian National Agency of Petroleum, Natural Gas, and Biofuels) and Petrobras (Brazilian National Oil Company) for the data set.

Author contributions Abel Carrasquilla: Conceptualization, methodology, software, validation, formal analysis, investigation, resources, data curation, writing—original draft, writing—review and editing, visualization, supervision, project administration, funding acquisition. Heitor Lichotti: Methodology, software, validation, formal analysis, investigation, data curation, writing—original draft, writing—review and editing, visualization. Herson Rocha: Conceptualization, methodology, validation, formal analysis, investigation, resources, data curation, writing—original draft, writing—review and editing, visualization, supervision.

Funding The Article Processing Charge (APC) for the publication of this research was funded by the Coordenação de Aperfeiçoamento de Pessoal de Nível Superior - Brasil (CAPES) (ROR identifier: 00x0ma614).

Data availability No datasets were generated or analysed during the current study.

Declarations

Conflict of interest The authors declare no competing interests.

Ethical approval Not applicable.

Consent to participate Not applicable.

Consent for publication The authors give consent to publish.

References

Aguilera R (2002) Incorporating capillary pressure, pore aperture radii, height above free water table, and Winland r35 values on Pickett plots. AAPG Bull 86(4):605–624. https://doi.org/10.1306/61EEDB5C-173E-11D7-8645000102C1865D

Akmal L, Pyrcz MJ (2025) Physics-based discrepancy modeling for well log imputation. Math Geosci 57(7):1235–1264. https://doi.org/10.1007/s11004-025-10203-7

Al Khalifah H, Glover P, Lorinczi P (2020) Permeability prediction and diagenesis in tight carbonates using machine learning techniques. Mar Pet Geol 112:104096. https://doi.org/10.1016/j.marpetgeo.2019.104096

Alizadeh N, Rahmati N, Najafi A, Leung E, Adabnezhad P (2022) A novel approach by integrating the core derived FZI and well logging data into artificial neural network model for improved permeability prediction in a heterogeneous gas reservoir. J Pet Sci Eng 214:110573. https://doi.org/10.1016/j.petrol.2022.110573

Al-Tooqi S, Ehrenberg S, Al-Habsi N, Al-Shukaili M (2014) Reservoir rock typing of upper Shu'aiba limestones, Northwestern Oman. Pet Geol 20(4):339–352. https://doi.org/10.1144/petgeo2014-024

Amaefule J, Altunbay M, Tiab D, Kersey D, Keelan D (1993) Enhanced reservoir description: using core and log data to identify hydraulic flow units and predict permeability in uncored intervals/wells. In: SPE annual technical conference and exhibition, Houston, pp 205–220. https://doi.org/10.2118/26436-MS

Beiranvand B, Ahmadi A, Sharafodin M (2007) Mapping and classifying flow units in the upper part of the mid-Cretaceous Sarvak formation (Western Dezful Embayment, Sw Iran) based on a determination of reservoir rock types. J Pet Geol 30(4):357–373. https://doi.org/10.1111/j.1747-5457.2007.00357.x

Brazilian National Agency of Petroleum, Natural Gas, and Biofuels (ANP) (2019) National Agency of Petroleum, Natural Gas and Biofuels. Bulletin of oil and natural gas production, external circulation, No. 101, development and production superintendence (SDP), Rio de Janeiro, p 32 **(in Portuguese)**

Brazilian National Oil Company (Petrobras) (2012) Oilfield a report, Petrobras—UENF Agreement, pp 150 **(in Portuguese)**

Bruhn C, Gomes J, Lucchese Jr C, Johann P (2003) Campos Basin: reservoir characterization and management-historical overview and future challenges. In: Offshore technology conference. Paper OTC 15220. https://doi.org/10.4043/15220-MS

Carrasquilla AG, Abreu C (2023) Estimation of the size and type of porosity in an Albian carbonate reservoir of the Campos Basin, Southeastern Brazil. Russ Geol Geophys 64(1):123–132. https://doi.org/10.2113/RGG20214382

Carrasquilla A, Rocha H (2025) Enhanced clustering techniques for lithofacies and electrofacies identification in post-salt carbonate and siliciclastic reservoirs: a case study from the Campos Basin, Brazil. Unconv Resour. https://doi.org/10.1016/j.uncres.2025.100211

Carrasquilla A, Silva R (2019) A petrophysical multivariate approach using geophysical well logs and laboratory measurements to characterize an Albian carbonate reservoir in the Campos Basin, Southeast Brazil. In: McNeill DF, Harris PM, Rankey EC, Hsieh JC (eds) Carbonate pore systems: new developments and case studies. SEPM Society for Sedimentary Geology. https://doi.org/10.2110/sepmsp.112.08

Da Costa JLS, Carrasquilla AAG, Carrasco AMV, da Rocha HO (2019) Forward modeling of electric and electromagnetic resistive logs with piston and annular invasion types in pre-salt carbonate reservoirs of the Santos Basin, Brazil. J Pet Sci Eng 178:216–226. https://doi.org/10.1016/j.petrol.2019.03.038

Dunham R (1962) Classification of carbonate rocks according to depositional textures. AAPG Special Volumes, Tulsa, OK, USA, pp 108–121

Formoso M, Robalna I, Spadlnl A (1991) Carbonate reservoir of the Macae Formation, Campos Basin, RJ, Brazil. Part I—contribution to the geochemistry of carbonates. Geochim Bras 5(1) **(in Portuguese)**

Geoactive (2023) IP: interactive petrophysics, version 5.1, Online user's manual. www.geoactive.com

Gomaa N, Azer S, Ouzzane D, Saif O, Okuyiga M, Allen D, Rose D, Ramamoorthy R, Bize E (2006) Case study of permeability, VUG quantification, and rock typing in a complex carbonate. In: SPE annual technical conference and exhibition, Santo Antonio, paper 102888, MS. https://doi.org/10.2118/102888-MS

Gomes J, Ribeiro M, Strohmenger C, Naghban S, Kalam M (2008) Carbonate reservoir rock typing—the link between geology and SCAL. In: SPE Abu Dhabi international petroleum exhibition and conference, paper 118284-MS. https://doi.org/10.2118/118284-MS

Gunter G, Finneran J, Hartman D, Miller J (1997) Early determination of reservoir flow units using an integrated petrophysical method. In: SSPE annual technical conference and exhibition, San Antonio, TX, paper SPE 38679. https://doi.org/10.2118/38679-MS

Hollis C, Vahrenkamp V, Tull S, Mookerjee A, Taberner C, Huang Y (2010) Pore system characterization in heterogeneous carbonates: an alternative approach to widely—used rock-typing methodologies. Mar Pet Geol 27(4):772–793. https://doi.org/10.1016/j.marpetgeo.2009.12.002

Jooybari H, Movazi G, Jaberi R (2010) A new approach for rock typing used in one of the Iranian carbonate reservoirs (a case study). In: SPE international oil and gas conference and exhibition, Beijing, paper 131915-MS. https://doi.org/10.2118/131915-MS

Khalid M, Desouky SE-D, Rashed M, Shazly T, Sediek K (2020) Application of hydraulic flow units' approach for improving reservoir characterization and predicting permeability. J Pet Explor Prod Technol 10(2):467–479. https://doi.org/10.1007/s13202-019-00758-7

Khalid MS, Mansour AS, Desouky SE-DM, Afify WS, Ahmed SF, Elnaggar OM (2024) Improving permeability prediction via machine learning in a heterogeneous carbonate reservoir: application to Middle Miocene Nullipore, Ras Fanar field, Gulf of Suez, Egypt. Environ Earth Sci 83(8):244. https://doi.org/10.1007/s12665-024-11534-0

Lichotti H (2016) Characterization of a carbonate reservoir in the Campos Basin based on the integration of geological attributes, petrophysical properties, and well log studies. Master's thesis, UENF/LENEP, Macae, RJ, Brazil, p 122 **(in Portuguese)**

Lucia J (2007) Carbonate reservoir characterization: an integrated approach. Springer, Berlin, Heidelberg, p 3434

Lucia FJ, Kerans C, Jennings JWJ (2003) Carbonate reservoir characterization. J Pet Technol 55(06):70–72. https://doi.org/10.2118/82071-JPT
Matlab (2021) User's manual. www.mathworks.com
Mehrabi H, Ranjbar-Karami R, Roshani-Nejad M (2019) Reservoir rock typing and zonation in sequence stratigraphic framework of the Cretaceous Dariyan Formation, Persian Gulf. Carbonates Evaporites. https://doi.org/10.1007/s13146-019-00530-2
Nugent W (1984) Letters to the editor. Log Anal 25(2):2–3. https://doi.org/10.2118/35160-MS
Okubo J, Lykawka R, Warren L, Favoreto J, Brito D (2015) Depositional, diagenetic, and stratigraphic aspects of Macae Group carbonates (Albian): an example from an oilfield from Campos Basin. Braz J Geol 45(2):243–258. https://doi.org/10.1590/23174889201500020005
Omeje E, Obiora D, Okeke F, Ugbor D, Ibuot J, Akpan A (2022) Aquifer flow unit analysis using stratigraphic modified Lorenz plot: a case study of Edem, eastern Nigeria. J Eng Appl Sci 69(33):1–13. https://doi.org/10.1186/s44147-022-00081-9
Penna R, Lupinacci W (2020) Decameter-scale flow-unit classification in Brazilian presalt carbonates. SPE Res Eval Eng 23(2020):1420–1439. https://doi.org/10.2118/201235-PA
Penna R, Lupinacci W (2021) 3D modelling of flow units and petrophysical properties in Brazilian presalt carbonate. Mar Pet Geol 124:104829. https://doi.org/10.1016/j.marpetgeo.2020.104829
Pittman E (1992) Relationship of porosity to permeability to various parameters derived from mercury injection-capillary pressure curves for sandstone. AAPG Bull 76(2):191–198. https://doi.org/10.1306/BDFF87A4-1718-11D7-8645000102C1865D
Rebelo T, Batezelli A, Mattos N, Leite E (2022) Flow units in complex carbonate reservoirs: a study case of the Brazilian pre-salt. Mar Pet Geol 140:105639. https://doi.org/10.1016/j.marpetgeo.2022.105639
Rocha HO, Moraes PEF, Carrasquilla AAG, de Figueiredo JJ (2025) Petrography image segmentation for analyzing the connectivity of pore networks in Brazilian pre-salt carbonate rocks of the Barra Velha Formation. Carbonates Evaporites 40(2):56. https://doi.org/10.1007/s13146-025-01084-2
Skalinski M, Kenter J (2015) Carbonate petrophysical rock typing: integrating geological attributes and petrophysical properties while linking with dynamic behaviour. Geol Soc Lond Spec Publ Geol Soc Lond 406(1):229–259. https://doi.org/10.1144/SP406.6
Tiab D, Donaldson E (2015) Petrophysics: theory and practice of measuring reservoir rock and fluid transport properties, 4th edn. Elsevier, Amsterdam, p 918
Timur A (1968) An investigation of permeability, porosity, and residual water saturation relationships for sandstone reservoirs. Log Anal 9(4):8–17
Winland H (1972) Oil accumulation in response to pore size changes, Weyburn field. Amoco Production Company, Saskatchewan. Report F72-G-25, p 20
Xu P, Zhou H, Liu X, Chen L, Xiong C, Lyu F, Zhou J, Liu J (2023) Permeability prediction using logging data in a heterogeneous carbonate reservoir: a new self-adaptive predictor. Geoenergy Sci Eng 224:211635. https://doi.org/10.1016/j.geoen.2023.211635
Zeitoum N, Vidal A, Ruidiaz E, de Almeida R (2024) Petrographical and petrophysical characterization of pre-salt Aptian carbonate reservoirs from the Santos Basin, Brazil. Pet Geosci. https://doi.org/10.1144/petgeo2023-045

Authors and Affiliations

Abel Carrasquilla[1] · Heitor Lichotti[1] · Herson Rocha[2]

✉ Herson Rocha
herson.rocha@macae.ufrj.br

[1] Petroleum Engineering and Exploration Laboratory (LENEP), Darcy Ribeiro Northern Rio de Janeiro State University (UENF), Macaé, Rio de Janeiro 27925-310, Brazil

[2] Polytechnic Institute (IPOLI), Federal University of Rio de Janeiro (UFRJ), Macaé, Rio de Janeiro 27930-560, Brazil